

Wafer-Scale Epitaxial Positioning of Quantum Dots

N. Bart^{1*}, C. Dangel^{2,3*}, P. Zajac¹, N. Spitzer¹, J. Ritzmann¹, M. Schmidt¹, K. Müller^{3,4},
A. D. Wieck¹, J.J. Finley^{2,3}, and A. Ludwig^{1†}

*1 - Ruhr-Universität Bochum, Lehrstuhl für Angewandte Festkörperphysik, Universitätsstraße 150, 44801
Bochum, Germany*

*2 – Walter Schottky Institut and Physik Department, Technische Universität München, Am Coulombwall 4,
85748 Garching, Germany*

3 - Munich Center for Quantum Science and Technology (MCQST), Schellingstr. 4, 80799 Munich, Germany

*4 - Walter Schottky Institut and Department of Electrical and Computer Engineering, Technische Universität
München, Am Coulombwall 4, 85748 Garching, Germany*

*These authors contributed equally to this work

†Correspondence to: Arne.Ludwig@rub.de

Control of the position and density of semiconductor quantum dots (QDs) is vital for a variety of emergent technologies, such as quantum photonics and advanced optoelectronic devices¹. However, established ordering methods typically call for ex-situ processing prior to growth that have a deleterious impact on the optical quality of nanostructures². Here, we apply a conventional epitaxial growth method – molecular beam epitaxy (MBE) – to achieve wafer scale positioning of optically active QDs with high reproducibility, tunable periodicity, and controlled density across an entire unpatterned 3-inch semiconductor wafer. Hereby, we exploit material thickness gradients across the wafer to modulate the QD nucleation probability and demonstrate how our approaches can be used to achieve strong periodic modulation of the local dot density tunable over length scales ranging from a few millimeters to at least a few hundred microns in one or two spatial directions. The methods are universal and are applicable to a wide variety of semiconductor material systems.

Spontaneous pattern formation is common in many natural systems having characteristic length scales ranging from the atomic to the cosmic scale. Typically, spontaneous ordering arises in inherently nonlinear systems due to the complex interplay of thermodynamic and dissipative processes leading to minimization of local free energies³. In the context of the lattice-mismatched growth of III-V semiconductor nanostructures, this principle is exploited to create defect free nanoscale islands of low bandgap materials surrounded by a wider bandgap matrix – self-assembled quantum dots (QDs). Such nanostructures are versatile building blocks for photonic device technologies, such as LEDs⁴, highly performant nanolasers⁵, or even as non-classical light sources for use in photonic quantum technologies¹. Key factors for the device integration of such QDs are their size, positioning at a relevant interaction length scales of the system and their local areal density⁶. For example, exploiting their narrow emission linewidth for modal gain in nano-lasers requires high density regions⁷,

whereas in quantum technology, highly-efficient single photon sources need low density and positioning over the length scale of the optical wavelength⁸. The growth mechanism of self-assembled QDs is based on strain relaxation during heteroepitaxy: Strain-energy builds up during the lattice mismatched growth between the substrate and deposited layer, inducing a change of growth mode from layer-by-layer growth (Frank van der Merwe) to layer-plus-island Stranski-Krastanov (SK) growth^{9,10}.

Due to random adatom arrival and diffusion, this nucleation process has a statistical nature and frequently leads to a random QD distribution over the substrate. In-situ techniques that achieved deterministic QD placement include the deposition through a shadow mask¹¹, changing the local diffusion length by laser heating¹², or hole-pattern formation by focused ion beam milling¹³. These approaches have the drawback of requiring complex pre-processing steps with significant setup modifications, and in the latter case, the difficulty of upscaling to a full semiconductor wafer. Ex-situ techniques encompass patterning by optical lithography¹⁴, electron beam writing¹⁵, or subsurface stressors¹⁶. These approaches frequently lead to the incorporation of impurities and creation of crystal defects². As such, key quantum-optical properties, such as near-unity indistinguishability and quantum efficiency, have all been demonstrated using randomly nucleated self-assembled QDs (see ref 1 and references therein). Purely in-situ processes that use conventional semiconductor growth methods and make use of self-assembly and self-positioning concepts would be game-changing.

Here, we introduce an alignment method that exploits spatially controllable substrate surface roughness to create preferential QD nucleation spots on non-patterned substrates during epitaxial growth. Compared to atomically smooth surfaces, QD nucleation is enhanced on rough surfaces^{14,17}. This is achieved by growing layer thickness gradients preceding the deposition of QD forming material. By controlling (i) the position of the cell relative to the substrate, (ii) the deposition time and (iii) the substrate temperature during and after growth,

we show that the roughness distribution can be engineered to produce a variety of QD density patterns on the wafer in one and two-dimensions.

All samples were grown on (100) surfaces of 3" GaAs wafers with no intentional miscut ($< 0.1^\circ$) in an ultra-high vacuum ($< 10^{-10}$ mbar) MBE system. We created a pattern defining layer (PDL) by growing GaAs from an inclined effusion cell at 600 °C substrate temperature while substrate rotation is stopped. Self-assembled QDs were then grown on top of the PDL at a substrate temperature of 525 °C and capped with GaAs¹⁸. Figure 1 shows typical photoluminescence (PL) intensity maps recorded from three different samples for which we smoothed the PDL for a time $t_{\text{smooth}} = 600$ s, 210 s and 0 s, respectively, before the substrate temperature was reduced for QD deposition. The example spectrum in fig. 1 shows three distinct QD emission peaks, corresponding to the ground state and the first two excited states, and the InAs wetting layer (WL) emission. The maps show the spectrally integrated emission intensity obtained from the QDs and WL of the highlighted spectral windows, respectively. Other than the inherent indium cell flux distribution, we observe no intensity modulation for $t_{\text{smooth}} = 600$ s. In contrast, a gradual spatial modulation of the intensity becomes visible after reducing t_{smooth} to 210 s. Finally, strong intensity modulations appear when smoothing is omitted altogether. Highest local contrasts are achieved for regions at the onset of QD formation (c.f. Supplementary Information) where the density varies from zero to finite values defined by the local coverage. Profile scans of the QD (WL) maps along the red (blue) dashed line show a homogeneous distribution of QDs and WL for the longest t_{smooth} , and a modulation of the intensities for the partially and non-smoothed samples. We observe an anti-correlation in the WL and QD emission intensity, suggesting that the QD density is varied rather than a global reduction of the quantum efficiency. This expectation is confirmed below by our correlated capacitance-voltage, atomic-force microscopy and spatially resolved luminescence measurements.

In contrast to the mechanism found in vicinal substrates QD patterning¹⁹, we rule out mass transport and alignment along steps, due to the large modulation period of 3 mm. Rather, we suggest a link between the local surface roughness on the wafer and QD density, as the disappearance of QD density modulation for a smoothing time of 600 s is comparable to the coalescence time of surface islands and holes as reported by Franke et al.²⁰.

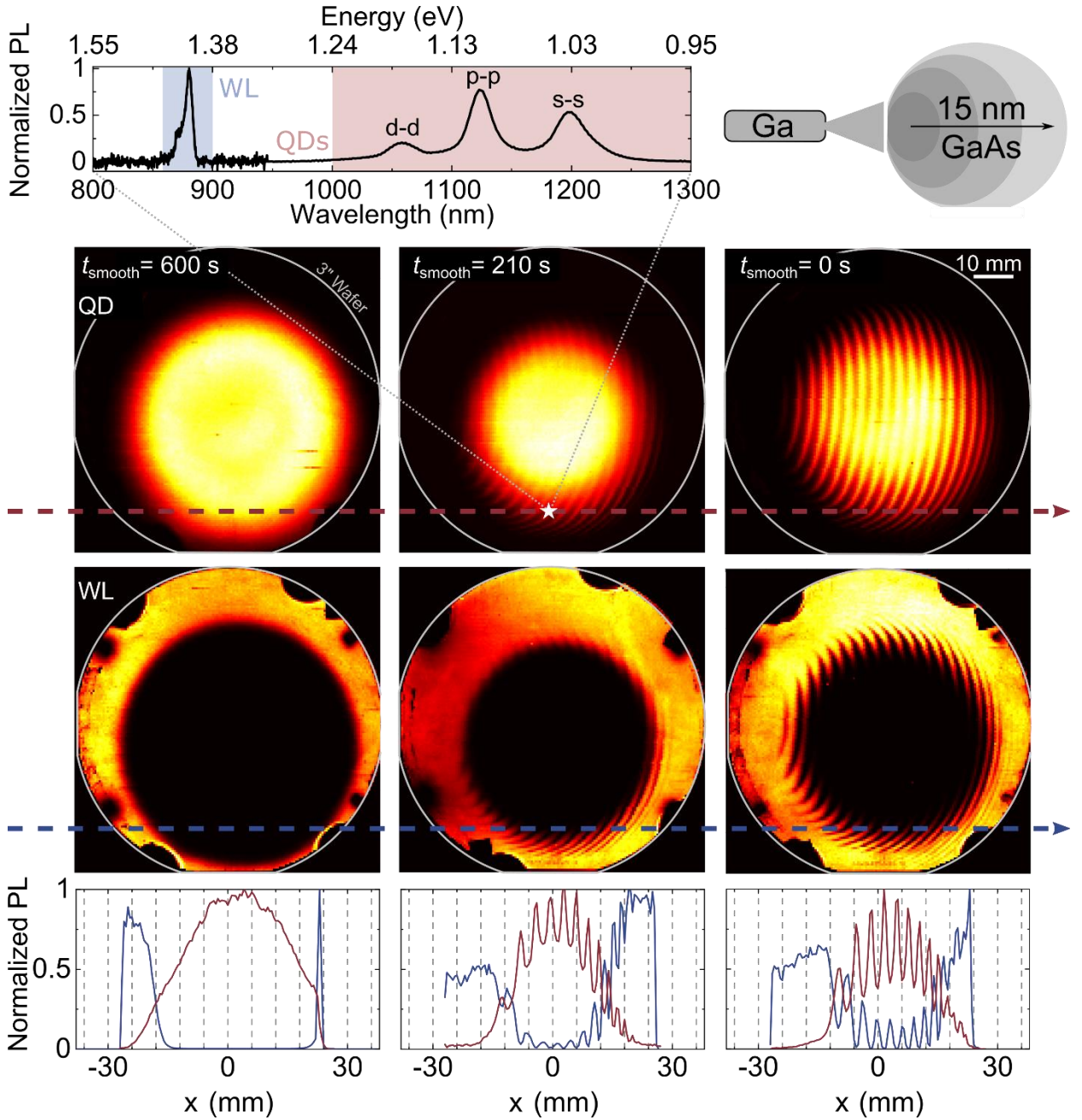


Fig. 1 | Effect of smoothing time on preferential nanostructure nucleation. Photoluminescence (PL) measurements at 77 K of 3" wafers with a nominally 15 nm thick GaAs pattern defining layer (PDL) are shown. The PL spectrum is recorded from the 210 s annealed sample (white star) and the

different peaks correspond to the different dipole and parity allowed interband transitions between orbital states and the wetting layer (WL) recombination. In the false color images the quantum dot (QD) PL intensity is spectrally integrated from 1000 to 1300 nm and the wetting layer (WL) emission from 860 to 900 nm. The wafers were smoothed before QD growth for 600 s, 210 s and 0 s, respectively. Profile scans show the recorded QD (WL) PL intensity along the dashed red (blue) line.

We developed a simple model to describe our experimental results based on strain relaxation during heteroepitaxy on surfaces that exhibit monolayer (ML) roughness. Despite its simplicity, we demonstrate below that this model produces remarkable agreement with our experimental results. Figure 2a shows the geometrical positioning of the effusion cell relative to the substrate. The distance and inclination angle of the cell, as well as deviations of the effusion profile from a point source result in inhomogeneities in the material deposition on the substrate^{21,22}. This undesired effect is usually counteracted by substrate rotation and smoothing breaks during layer growth²³. As illustrated in fig. 2a, layer growth without substrate rotation results in a significant difference in total layer thickness across the wafer. In this work, a typical GaAs gradient layer consists of a nominal thickness of 15 nm, corresponding to a 22 ML (~6 nm) thickness difference across the wafer from the side farthest from the cell, to the side nearest. A surface is atomically smooth (rough) when an integer (fractional) number of monolayers has been deposited²⁴. Heyn et al.²⁵ have shown that after GaAs homoepitaxy on a smooth surface, the new surface needs a certain time, depending on the temperature, to recover smoothness. Here, we decrease the substrate temperature quickly after deposition of a GaAs gradient layer to prevent GaAs smoothing, leaving the surface morphology in its current state, and therefore exhibiting local roughness modulations across the wafer.

Leonard et al.¹⁰ have shown that QDs start nucleating above a critical layer thickness $\Theta_c = 1.5$ ML of InAs for smooth substrates. As illustrated in fig. 2b, a rough surface provides

atom-scale disorders²⁰, which act as traps for diffusing In adatoms resulting in accumulation of material²⁶. This leads to preferential nucleation of QDs at these rough areas, as the critical layer thickness is exceeded locally.

Motivated by these ideas, in fig. 2c we present simulations of the distribution of the QD density in which θ_c is a function of a dimensionless roughness parameter $R(\theta_{\text{PDL}}) = \gamma \cdot \sin^2\left(\pi \cdot \frac{\theta_{\text{PDL}}}{\text{ML}}\right)$, that varies sinusoidally between an arbitrarily defined base roughness zero for full monolayer and $R_{\text{max}} = \gamma$ for half monolayer coverage of the locally deposited PDL thickness θ_{PDL} . We propose a simple linear modulation of the critical thickness by this roughness parameter according to

$$\theta_c^{\text{mod}}(R) = \theta_c (1 - R).$$

Using growth rates deduced by the evaluation of quantum well emission energies and including the geometry of the effusion cell relative to the substrate, we simulate the growth of a 15 nm GaAs PDL followed by nominally ~ 1.7 ML of InAs in the wafer center as the dot layer, where we observe a clear modulation of density comparing well to the experimental maps presented in fig. 1.

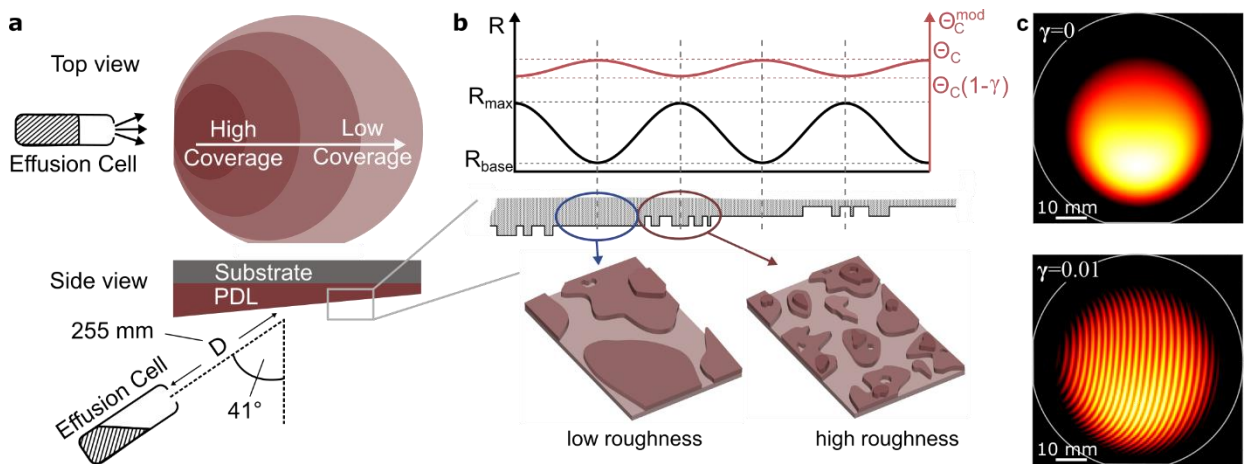


Fig. 2 | Growth geometry and suggested model. **a**, Schematic representation of the gradient of material coverage on the substrate in top view (top) and geometrical configuration inside the MBE growth chamber viewed from the side (bottom). **b**, Proposed surface morphology and roughness

modulation after deposition of the pattern defining layer (PDL) exhibiting areas with high and low atomic level roughness. **c**, Simulation results of QD density using no variation of the roughness (top) and modulated roughness (bottom).

To confirm the model of local surface roughness modulation being responsible for our observed periodic dot nucleation, we analyzed the morphology of a 15 nm gradient grown GaAs surface PDL using atomic force microscopy (AFM). Figure 3a,b compares an AFM scan of a smooth to a rough location, with a clearly observable decrease of the average island and hole size. In figure 3c, we find a clear modulation in the density of atomic steps along the gradient direction between 5 and 7 steps per μm . The observed modulation period of ~ 3 mm is in excellent accordance with the spatially dependent PL measurements presented in fig. 1.

To link PL intensity variations to the density of QDs, we performed capacitance-voltage (C-V) spectroscopy. In figure 3d we present typical measurements of two charging peaks of a first and a second electron in each QD of a Schottky diode sample, recorded from devices fabricated at locations between lowest and highest QD densities ρ_{QD} . C(V) integrated over the voltage range corresponding to the inhomogeneously broadened charging peak increases as an increasing number of QDs can be charged. ρ_{QD} extracted from this are plotted in fig. 3e along with the PL intensity at these locations. The local QD densities at this specific area on the wafer, obtained using C-V spectroscopy, range from $4 \mu\text{m}^{-2}$ to $11 \mu\text{m}^{-2}$, corresponding to a variation of the parameters θ_c by 0.023 ML or $\gamma = 0.015$ as defined in our model above.

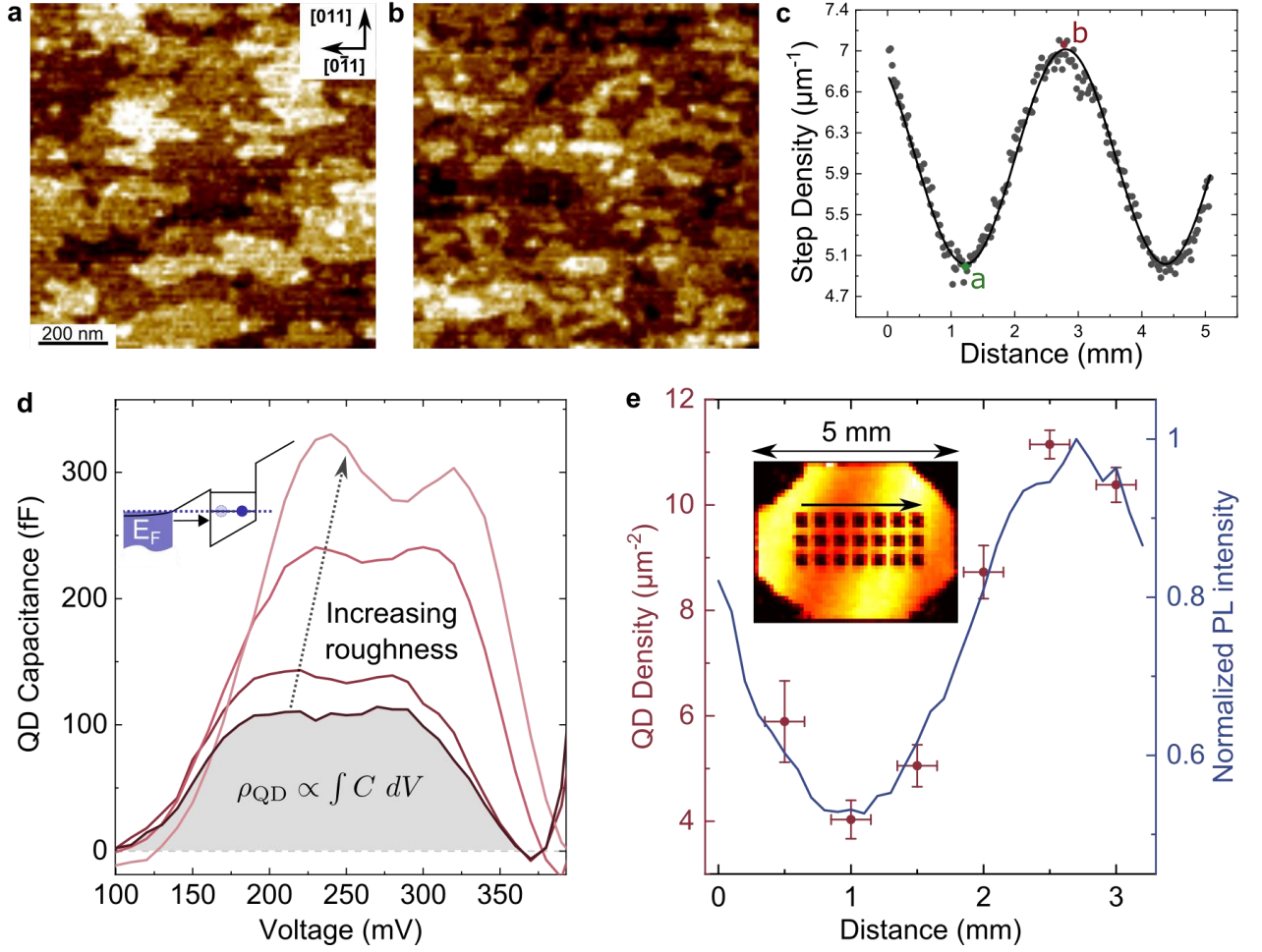


Fig. 3 | Surface roughness and QD density. AFM measurements along a non-buried GaAs gradient, where **a**, **(b)** shows a smooth (rough) region with a low (high) number of atomic steps. **c**, Number of steps per μm in $[0\bar{1}1]$ direction. **d**, Capacitance-Voltage spectroscopy of buried QDs along the roughness modulation. The inset shows a sketch of the sample bandstructure at a voltage, where electrons can tunnel from the Fermi level of the n-doped back contact E_F to the QD ground state. **e**, QD densities deduced by C-V spectroscopy and PL intensity are plotted versus distance on the sample. The inset shows a PL map of the processed area. Black regions are metallization of the back-contacts in the corners and Schottky-gates, respectively.

We continue to demonstrate control over the pattern formation along different axes on the 3-inch wafer by showing how modulation of the QD density along a single direction can be transformed into two-dimensional control. Figure 4 shows how the modulation period can be controlled by tailoring the nominal gradient thickness: By doubling the PDL thickness from 15 nm to 30 nm, the modulation period is halved from 3 mm to 1.5 mm. Comparing PL maps in fig. 1 to the PL map of the 30 nm sample in fig. 4, we demonstrate full wafer-scale modulation of the QD density by increasing the InAs amount. Analyzing the PL maps

provides a way to easily measure the PDL cell effusion profile with sub-monolayer precision across the entire wafer, as the QD intensity modulation is directly correlated to deposited monolayers.

The next column of fig. 4 shows how increasing the PDL thickness by a factor of ten to 150 nm, from the 15 nm thick PDL, decreases the modulation period to 300 μm . It becomes evident that even for more than 500 deposited monolayers, the roughness modulation is preserved at the growth surface. Moreover, in the sample presented in fig. 4 we changed the PDL material from GaAs to a ternary $\text{Al}_{33}\text{Ga}_{67}\text{As}$ alloy, demonstrating that PDL growth is not limited to binary alloys such as GaAs. In the sample presented in fig. 4, before QD growth we added a 2.5 nm GaAs buffer layer for non-GaAs PDLs, which inherits the underlying PDL roughness modulation. As can be seen in supplementary fig. 1c, we observe this even with a pure AlAs PDL.

Finally, in the rightmost column of fig. 4 we demonstrate that our methods can be used to modulate the density of QDs in a 2D lattice on the sample surface. We first grow an 80 nm thick PDL to define a specific axis along which the density is modulated, followed by a 60 s smoothing growth interruption before growing a second 40 nm PDL along an axis orientated at a relative angle of 120° to the first. The smoothing growth interruption between the growth of the two PDLs is necessary to provide partially smooth areas interspersed in rough regions for the second layer modulation while still retaining some of the roughness modulation of the first layer. We performed simulations of the local QD density using our model and obtained results that very closely resemble the measured data. This observation clearly shows that our methods are highly flexible allowing design of a specific 2D pattern across the entire wafer before QD growth. Here, the images presented in fig. 4 were obtained by simulating the grown layer sequences and a roughness scaling factor $\gamma = 0.01$. For single PDLs, the simulated roughness follows from the deposited thickness profiles. For a combination of more

than one PDL, as is the case for example for a 2D grid, the individual roughness modulations for each PDL are calculated and summed to obtain the overall roughness profile.

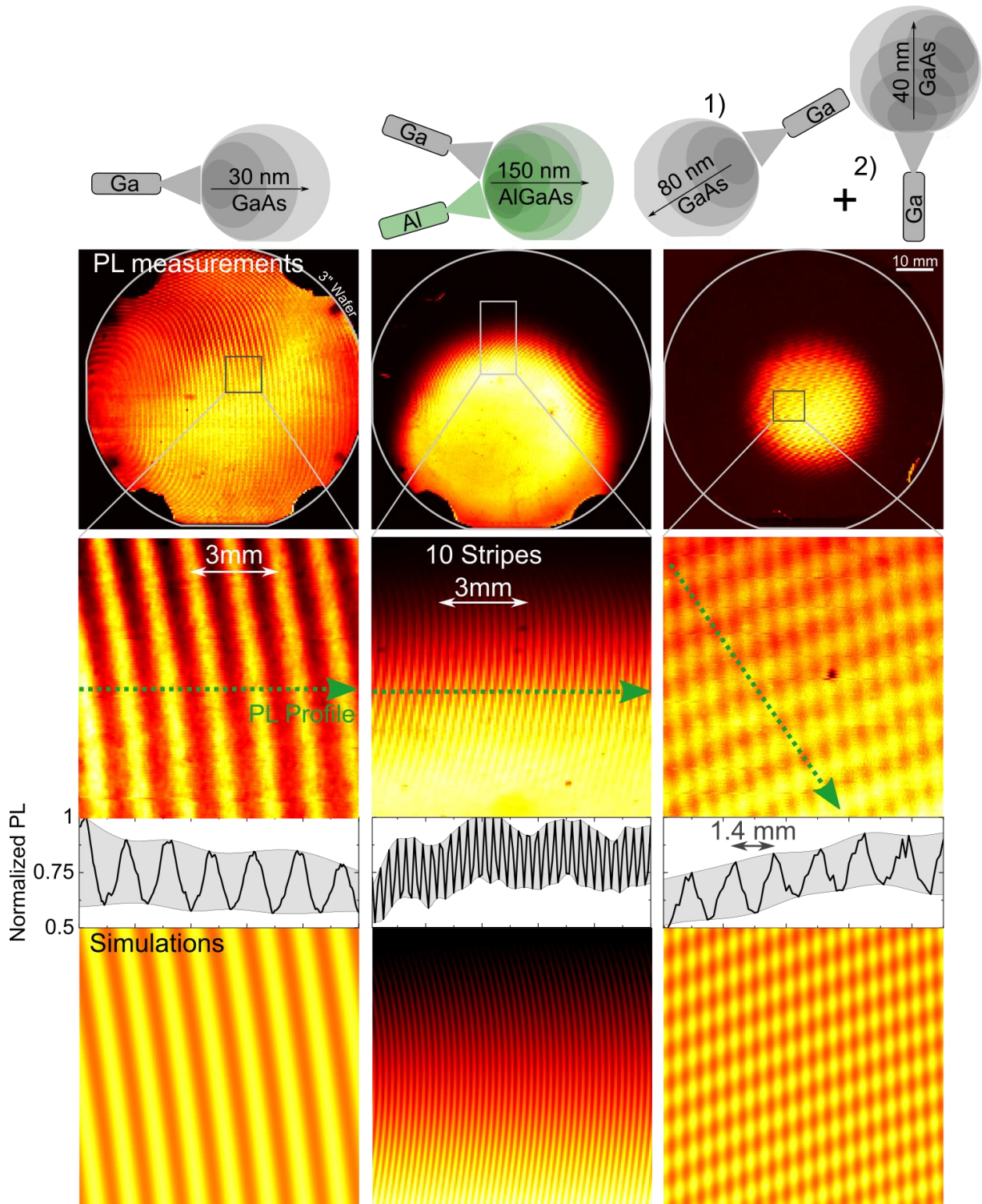


Fig. 4 | Demonstration of pattern control. QD PL intensity maps of 30 nm GaAs PDL (left column), 150 nm AlGaAs PDL (middle column) and superposition of 80 and 40 nm GaAs PDL. White/yellow indicate high intensity, red/black low. High resolution maps of the marked areas are shown below. The fourth row shows the PL intensity along the green dotted line of the respective zoom-in. The bottom row shows QD-density simulations of the respective zoom-in according to a geometric approach, yellow corresponds to high density, red to low density.

The data presented in fig. 4 clearly shows that spatial roughness modulation is universal to gradient layer-by-layer growth using any material or alloy in our group-III arsenide MBE. Thus, we conclude that the self-positioning method presented here for the first time could also be applied to other materials systems based on strain-driven self-assembly⁹. Beyond this, first growth trials using our MBE system hint towards ordering effects of metallic droplets on an AlGaAs PDL, which can be used for droplet epitaxy or hole etching and subsequent local droplet etch dot growth^{27,28}.

Smaller modulation periods than those presented in fig. 4 can be achieved by using even steeper gradients. In our simple rotation stop approach, this would require thick layers. However, a solution is a partial flux shadowing and creating steeper thickness variations. We anticipate that the physical limitation is defined by the point at which the Ga adatom diffusion length on GaAs (< 10 nm)²⁹ becomes comparable to the roughness modulation period. We note that it is likely that our PDL technique is not compatible with step-flow growth since no roughness undulations occur. However, due to the simplicity and robustness of the new positioning method presented in this paper, we believe that the results clearly demonstrate that low-cost devices using high quality self-assembled QD nanostructures are firmly within reach.

Acknowledgements

The authors wish to thank Florian Stumpf from Park Systems for performing AFM measurements.

We gratefully acknowledge support from the German Federal Ministry of Education and Research via the funding program Photonics Research Germany (contract number 13N14846, Q.Link.X Project 16KIS0874 and 16KIS0867). Moreover, C.D., K.M, J.J.F. gratefully

acknowledge the Deutsche Forschungsgemeinschaft (DFG, German Research Foundation) via Germany's Excellence Strategy – EXC-2111/1 – 390814868 and EXC-2089/1 – 390776260. J.J.F. gratefully acknowledges the DFG for funding via projects FI947-5, FI947-6 and INST 95-164. N.B., A.D.W., and A.L. acknowledge gratefully support of TRR 160/2-Project B04, DFG 383065199 and the DFH/UFA CDFA-05-06.

Competing interests

N.B., C.D., K.M., A.D.W., J.J.F., and A.L. applied for European patent under file number EP19177713.

Methods

Sample growth

All samples were grown on undoped (100) surfaces of 3" GaAs wafers with a miscut $<0.1^\circ$ (as specified by the vendor) using a Riber MBE System. Before growth, wafers are heated to 640°C under an As atmosphere of $9.6 \cdot 10^{-6}$ Torr beam equivalent pressure to remove surface oxides. We use growth rates of 0.2 nm/s for GaAs, 0.1 nm/s for AlAs and ~ 0.013 nm/s for InAs. We prepare the wafers by deposition of a buffer consisting of a 50 nm thick GaAs layer and a 30 period superlattice of 2 nm AlAs and 2 nm GaAs, followed by another 50 nm GaAs buffer layer. For electrical contact we grow a Si-doped back contact with a doping concentration of $2 \cdot 10^{18} \text{cm}^{-3}$. Next, a pattern defining layer (PDL) of GaAs, AlAs or a ternary alloy $\text{Al}_x\text{Ga}_{(1-x)}\text{As}$ was grown (see Supplementary Table 1). To avoid direct QD growth on ternary alloys, a 2.5 nm thick spacer layer of GaAs is deposited on the Al-

containing PDLs. Quantum dots are grown in SK-growth mode at 525 °C substrate temperature and an As BEP of $6.8 \cdot 10^{-6}$ Torr and are capped with a 10 nm thick layer of undoped GaAs, 130 nm AlGaAs and 5 nm GaAs. QDs in samples where the dot height was reduced to 3 nm due to the indium flushing method have an emission wavelength of 910 to 960 nm. For QD growth details refer to Ludwig et al.¹⁸.

Photoluminescence measurements

PL measurements were performed by exciting samples with a 518 nm laser with a spot size of $\sim 100 \mu\text{m}$ in diameter with powers between 1 and 20 mW. Liquid nitrogen was used to cool a 3" coldfinger inside a cryostat which is fixed to two stepping motors for position control. Thus, sample temperature for all PL measurements is approximately 100 K, except for PL measurements of fig. 3e, which are measured at room temperature. A Si-based spectrometer was used for measurement of wavelengths between 340 and 1020 nm, combined with an InGaAs linear array spectrometer for 900 to 1715 nm.

Atomic force microscopy

For atomic force microscopy (AFM) measurements, a Park Systems NX20 was used in non-contact mode. Areas of $5 \times 5 \mu\text{m}^2$ with a resolution of $512 \times 512 \text{ px}^2$ were scanned.

Capacitance-Voltage measurements

For Capacitance-Voltage (CV) measurements, n-i-Schottky diodes were used. The Schottky contacts are $300 \times 300 \mu\text{m}^2$ gold gates that are bonded inside a 16 pin carrier, using ultrasonic bonding. Measurements were performed at liquid Helium temperatures (4.2 K) using an ac voltage at 2333 Hz with 10 mV amplitude (rms) superimposed to a dc voltage (swept to align the band) and a lock-in amplifier. The QD density ρ_{QD} extracted from the background

subtracted capacitance C of the finite twofold degeneracy of the lowest energy orbital states is given by

$$\rho_{QD} = \frac{\lambda}{2e A_G} \int C dV$$

where λ is the ratio of the distances between the n-doped back contact and i) the Schottky gate and ii) the QDs, e the elementary charge, V the dc gate voltage and A_G the surface area of the gate³⁰.

References

- 1 Senellart, P., Solomon, G. & White, A. High-performance semiconductor quantum-dot single-photon sources. *Nat Nanotechnol* **12**, 1026-1039, doi:10.1038/nnano.2017.218 (2017).
- 2 Lan, H. & Ding, Y. Ordering, positioning and uniformity of quantum dot arrays. *Nano Today* **7**, 94-123 (2012).
- 3 Betzler, S. B. *et al.* Template-free synthesis of novel, highly-ordered 3D hierarchical Nb 3 O 7 (OH) superstructures with semiconductive and photoactive properties. *Journal of Materials Chemistry A* **2**, 12005-12013 (2014).
- 4 Liu, Z. *et al.* Micro-light-emitting diodes with quantum dots in display technology. *Light Sci Appl* **9**, 83, doi:10.1038/s41377-020-0268-1 (2020).
- 5 Strauf, S. & Jahnke, F. Single quantum dot nanolaser. *Laser & Photonics Reviews* **5**, 607-633, doi:10.1002/lpor.201000039 (2011).
- 6 Grydlik, M., Langer, G., Fromherz, T., Schaffler, F. & Brehm, M. Recipes for the fabrication of strictly ordered Ge islands on pit-patterned Si(001) substrates. *Nanotechnology* **24**, 105601, doi:10.1088/0957-4484/24/10/105601 (2013).
- 7 Kreinberg, S. *et al.* Emission from quantum-dot high-beta microcavities: transition from spontaneous emission to lasing and the effects of superradiant emitter coupling. *Light Sci Appl* **6**, e17030, doi:10.1038/lsa.2017.30 (2017).
- 8 Tomm, N. *et al.* A bright and fast source of coherent single photons. *arXiv preprint arXiv:2007.12654* (2020).
- 9 Sautter, K. E., Vallejo, K. D. & Simmonds, P. J. Strain-driven quantum dot self-assembly by molecular beam epitaxy. *Journal of Applied Physics* **128**, 031101 (2020).
- 10 Leonard, D., Pond, K. & Petroff, P. M. Critical layer thickness for self-assembled InAs islands on GaAs. *Phys Rev B Condens Matter* **50**, 11687-11692, doi:10.1103/physrevb.50.11687 (1994).
- 11 Zolatanosha, V. & Reuter, D. Site-controlled droplet epitaxy of GaAs quantum dots by deposition through shadow masks. *Journal of Vacuum Science & Technology B, Nanotechnology and Microelectronics: Materials, Processing, Measurement, and Phenomena* **36**, doi:10.1116/1.5013650 (2018).
- 12 Wang, Y. R., Han, I. S., Jin, C. Y. & Hopkinson, M. Precise Arrays of Epitaxial Quantum Dots Nucleated by In Situ Laser Interference for Quantum Information Technology Applications. *ACS Appl Nano Mater* **3**, 4739-4746, doi:10.1021/acsanm.0c00738 (2020).

- 13 Portavoce, A., Hull, R., Reuter, M. C. & Ross, F. M. Nanometer-scale control of single quantum dot nucleation through focused ion-beam implantation. *Physical Review B* **76**, doi:10.1103/PhysRevB.76.235301 (2007).
- 14 Wang, Z. M. *et al.* Localized formation of InAs quantum dots on shallow-patterned GaAs(100). *Applied Physics Letters* **88**, doi:10.1063/1.2209157 (2006).
- 15 Atkinson, P., Schmidt, O. G., Bremner, S. P. & Ritchie, D. A. Formation and ordering of epitaxial quantum dots. *Comptes Rendus Physique* **9**, 788-803, doi:10.1016/j.crhy.2008.10.014 (2008).
- 16 Nakamura, Y. *et al.* Vertical alignment of laterally ordered InAs and InGaAs quantum dot arrays on patterned (0 0 1) GaAs substrates. *Journal of crystal growth* **242**, 339-344 (2002).
- 17 Xu, M. C., Temko, Y., Suzuki, T. & Jacobi, K. On the location of InAs quantum dots on GaAs(001). *Surface Science* **589**, 91-97, doi:10.1016/j.susc.2005.05.052 (2005).
- 18 Ludwig, A. *et al.* Ultra-low charge and spin noise in self-assembled quantum dots. *Journal of Crystal Growth* **477**, 193-196 (2017).
- 19 Schmidbauer, M. *et al.* Controlling planar and vertical ordering in three-dimensional (In,Ga)As quantum dot lattices by GaAs surface orientation. *Phys Rev Lett* **96**, 066108, doi:10.1103/PhysRevLett.96.066108 (2006).
- 20 Franke, T., Kreutzer, P., Zacher, T., Naumann, W. & Anton, R. In situ RHEED, AFM, and REM investigations of the surface recovery of MBE-grown GaAs (0 0 1)-layers during growth interruptions. *Journal of crystal growth* **193**, 451-459 (1998).
- 21 Nanbu, K. & Watanabe, Y. Thickness distribution of films fabricated by the molecular beam epitaxy technique. *Vacuum* **36**, 349-354 (1986).
- 22 Yamashita, T., Tomita, T. & Sakurai, T. Calculations of molecular beam flux from liquid source. *Japanese journal of applied physics* **26**, 1192 (1987).
- 23 Park, C. Y., Kim, J. M., Park, K. W., Yu, J. S. & Lee, Y. T. Improvement of the optical property and uniformity of self-assembled InAs/InGaAs quantum dots by layer-by-layer temperature and substrate rotation. *Physica E: Low-dimensional Systems and Nanostructures* **40**, 3160-3165, doi:10.1016/j.physe.2008.05.014 (2008).
- 24 Joyce, B. *et al.* RHEED studies of heterojunction and quantum well formation during MBE growth—from multiple scattering to band offsets. *Surface Science* **168**, 423-438 (1986).
- 25 Heyn, C., Franke, T., Anton, R. & Harsdorff, M. Correlation between island-formation kinetics, surface roughening, and RHEED oscillation damping during GaAs homoepitaxy. *Physical Review B* **56**, 13483 (1997).
- 26 Toujyou, T. & Tsukamoto, S. In situ STM observation during InAs growth in nano holes at 300°C. *Surface Science* **605**, 1320-1323, doi:10.1016/j.susc.2011.04.026 (2011).
- 27 Gurioli, M., Wang, Z., Rastelli, A., Kuroda, T. & Sanguinetti, S. Droplet epitaxy of semiconductor nanostructures for quantum photonic devices. *Nature materials*, 1 (2019).
- 28 Zhai, L. *et al.* Low-noise GaAs quantum dots for quantum photonics. *Nature Communications* **11**, 4745, doi:10.1038/s41467-020-18625-z (2020).
- 29 Ohta, K., Kojima, T. & Nakagawa, T. Anisotropic surface migration of Ga atoms on GaAs (001). *Journal of Crystal Growth* **95**, 71-74 (1989).
- 30 Drexler, H., Leonard, D., Hansen, W., Kotthaus, J. P. & Petroff, P. M. Spectroscopy of quantum levels in charge-tunable InGaAs quantum dots. *Phys Rev Lett* **73**, 2252-2255, doi:10.1103/PhysRevLett.73.2252 (1994).

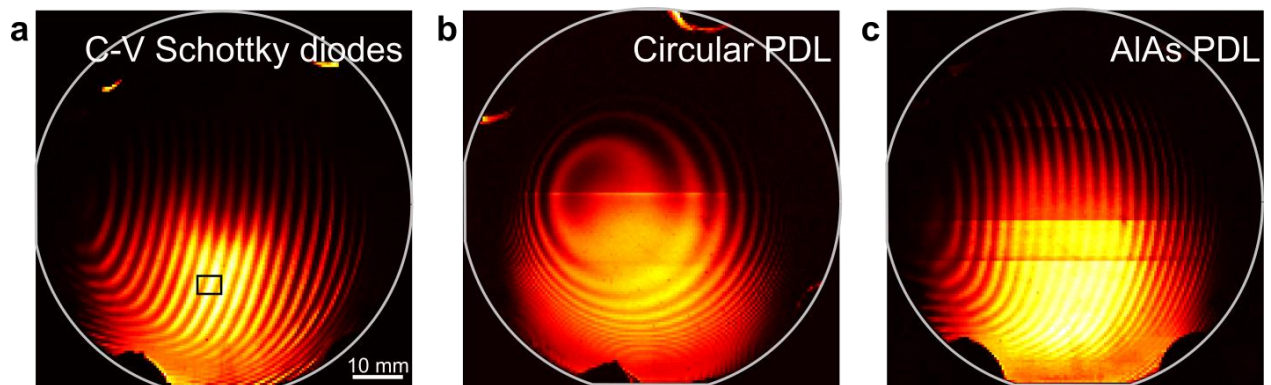
Supplementary Information to:

Wafer-Scale Epitaxial Positioning of Quantum Dots

Supplementary Table 1 | Overview of sample growth parameters.

Figure	PDL	PDL Temperature (°C)	Smoothing break (s)	Wafer size (")	Flushing height (nm)
1 (left)	15 nm GaAs	600	600	3	-
1 (middle)	15 nm GaAs	600	210	3	-
1 (right), S2	15 nm GaAs	600	0	3	-
3 (a-c)	15 nm GaAs	600	0	2	-
3 (d,e), S1 (a)	15 nm GaAs	525	30	3	3
5 (left)	30 nm GaAs	600	0	3	3
5 (middle)	150 nm Al ₃₃ Ga ₆₇ As + 2.5 nm GaAs	600	0	3	3
5 (right)	1) 80 nm GaAs, 2) 40 nm GaAs	600	1) 60, 2) 0	3	-
S1 (b)	75 nm Al ₃₃ Ga ₆₇ As + 2.5 nm	600	0	3	3
S1 (c)	15 nm AlAs + 2.5 nm GaAs	600	0	3	3
S3, S4	15 nm GaAs	600	0	3	-
S5	30 nm AlGaAs	630	30 + 120	3	-

Additional samples with different Al-concentration and geometry



Supplementary Fig. 1 | Photoluminescence measurements performed on additional samples. a, Sample wafer used for C-V measurement presented in Fig. 3 d,e. The CV data presented in Fig. 3 was recorded from Schottky photodiode samples processed from the marked region on the wafer. **b**, 75 nm thick Al₃₃Ga₆₇As PDL with wafer rotation resulting in a circular pattern. **c**, 15 nm thick AlAs PDL. Horizontal line discontinuities in the PL intensity maps originate from interrupted cooling during the line-scan PL map.

Generalized model for critical thickness modulation

In the following, we expand the proposed roughness model as presented in Fig. 2 to a generalized version.

We define a roughness modulated surface in agreement with AFM measurements, according to

$$R(\theta_{\text{PDL}}) = R_0 + \Delta R \cdot \sin^2 \left(\pi \cdot \frac{\theta_{\text{PDL}}}{\text{ML}} \right)$$

with a base roughness R_0 and a roughness amplitude ΔR in units of the roughness measurement method. Both parameters depend as well on material properties, and the locally deposited PDL thickness θ_{PDL} . Therefore, the roughness varies sinusoidally between R_0 and $R_0 + \Delta R$. We find a modulated critical thickness θ_c^{mod} according to

$$\theta_c^{\text{mod}}(R) = \theta_{c,0} \left(1 - \frac{R}{\eta} \right),$$

for an idealized perfectly smooth surface with a critical layer thickness $\theta_{c,0}$ and a conversion factor η associating the (measured) roughness modulation with the modulation in critical thickness. Accommodating for real surfaces, $\theta_{c,0}$ is reduced by the base roughness according to $\theta_c = \theta_{c,0} \left(1 - \frac{R_0}{\eta} \right)$. Incorporating this into the equation for θ_c^{mod} , we arrive at

$$\theta_c^{\text{mod}} = \theta_c \left(1 - \frac{\Delta R}{\eta - R_0} \sin^2 \left(\pi \frac{\theta_{\text{PDL}}}{\text{ML}} \right) \right),$$

to convert the measured surface roughness to a critical thickness modulation. The modulation magnitude is $\frac{\Delta R}{\eta - R_0} = \gamma$, as used in Fig. 2.

Close to the threshold for SK-growth the QD nucleation probability can be linked to the deposited InAs thickness θ according to the parametric relation¹:

$$\rho_{\text{QD}}(\theta) = \rho_0(\theta - \theta_c)^\alpha,$$

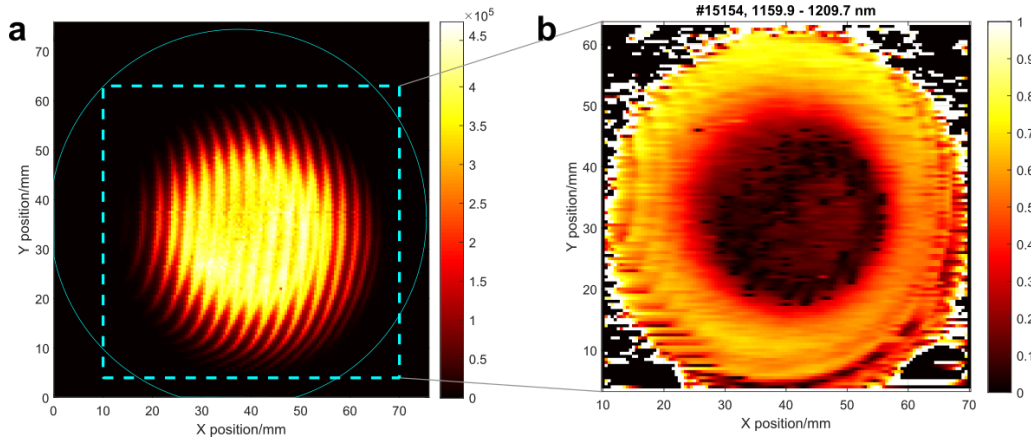
with ρ_{QD} being the QD density. According to Leonard et al.¹, $\rho_0 = 2 \cdot 10^{11} \text{ cm}^{-2}$ is the normalization QD density, $\theta_c = 1.5 \text{ ML}$ the critical thickness for QD nucleation and the exponent $\alpha = 1.76$ parametrizes the density above θ_c . Finally, substituting θ_c with θ_c^{mod} results in a modulated QD density ρ_{QD} .

Detailed study of local contrast

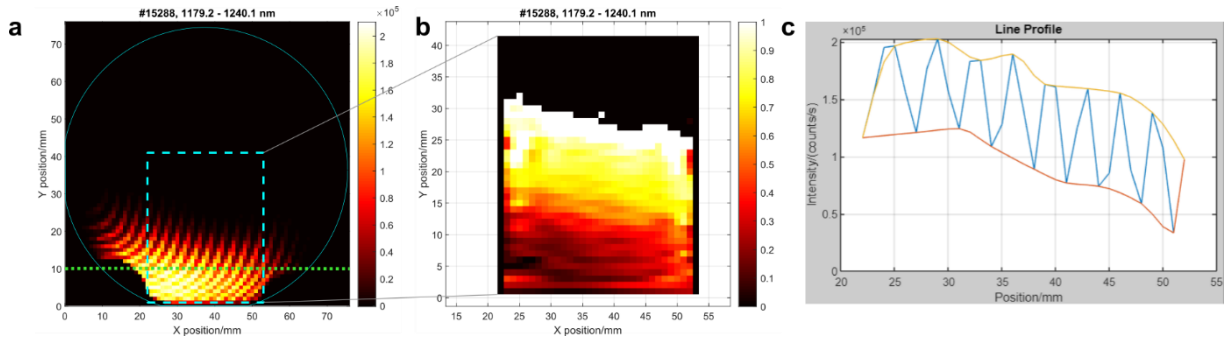
We define a Michelson-contrast in our photoluminescence (PL) maps by comparing spectrally integrated ranges for high and low intensity by creating envelope functions:

$$c_{\text{Michelson}} = \frac{I_{\text{high}} - I_{\text{low}}}{I_{\text{high}} + I_{\text{low}}},$$

with I_{high} the upper and I_{low} the lower envelope. In all samples, highest local contrast is found in regions with an InAs amount close to the critical amount θ_C .

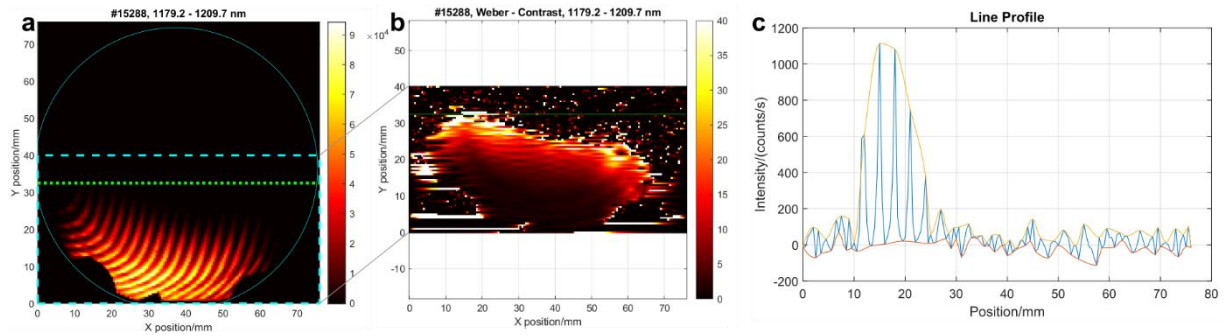


Supplementary Fig. 2 | Photoluminescence and Michelson-contrast for $t_{\text{smooth}} = 0$ s sample. a, PL map. **b**, Michelson contrast of the marked region in **a** (blue dashed box).



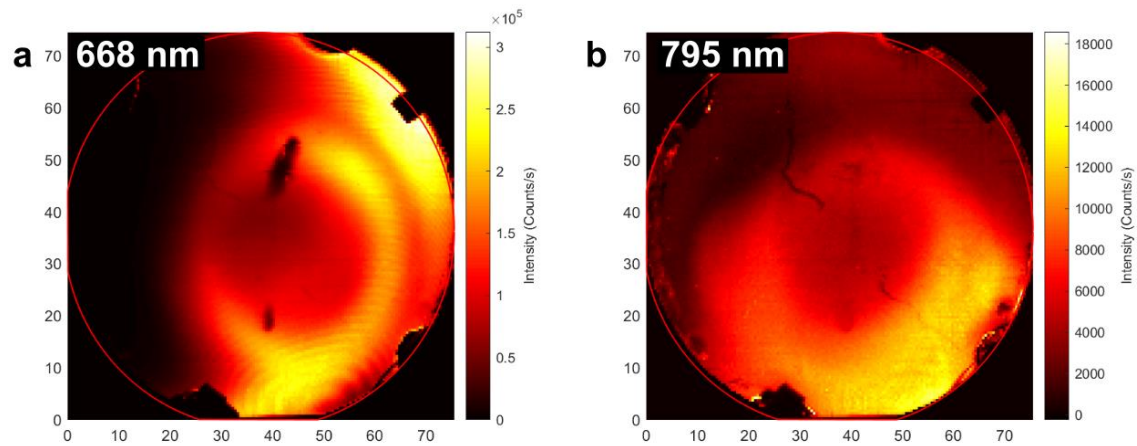
Supplementary Fig. 3 | Photoluminescence and Michelson-contrast for a high contrast sample. a, Full wafer PL map. **b**, Michelson-contrast of the marked region in **a** (blue dashed box). Note that the QD nucleation onset region is located at $y = 20$ - 30 mm, where due to scaling no luminescence is visible in **a**. **c**, PL intensity (blue line) along the green dotted line from subfigure **a** and upper (yellow) and lower (red) envelope functions.

For visualising high contrast values, the Weber-contrast $c_{\text{Weber}} = (I_{\text{high}} - I_{\text{low}}) / I_{\text{low}}$ is more useful. High Weber-contrasts $c_{\text{Weber}} > 100$ are found.



Supplementary Fig. 4 | Photoluminescence and Weber-contrast for a high contrast sample. **a**, Full wafer PL map. **b**, Weber-contrast of the marked region in **a** (blue dashed box). Note that the QD nucleation onset region is located at $y = 20\text{--}30\text{ mm}$, where due to scaling no luminescence is visible in **a**. **c**, PL intensity (blue line) along the green dotted line (at the onset of QD nucleation) from subfigure **a** and upper (yellow) and lower (red) envelope functions.

Hints of modulation of metallic local droplet etch dots



Supplementary Fig. 5 | Photoluminescence measurements performed on local Al droplet etch dots. **a**, PL map at 668 nm. **b**, PL map of the GaAs quantum dots at 795 nm in the same sample.

We grow an AlGaAs PDL with a nominal thickness of 30 nm at the centre of the wafer oriented from bottom right to top left. Despite local droplet etching being not a Stranski-Krastanov growth method, we find a faint modulation of the intensity in the PL map. Possible reasons for the weak contrast are a high growth temperature and long annealing breaks necessary for local droplet etch dot epitaxy after the PDL growth².

- 1 Leonard, D., Pond, K. & Petroff, P. M. Critical layer thickness for self-assembled InAs islands on GaAs. *Phys Rev B Condens Matter* **50**, 11687-11692, doi:10.1103/physrevb.50.11687 (1994).
- 2 Zhai, L. *et al.* Low-noise GaAs quantum dots for quantum photonics. *Nature Communications* **11**, 4745, doi:10.1038/s41467-020-18625-z (2020).